RSC Advances

RSC Publishing

PAPER

View Article Online
View Journal | View Issue

Far infrared response of silicon nanowire arrays

K. Fobelets,*[a] C. B. Li,[ab] D. Coquillat,[c] P. Arcade[c] and F. Teppe[c]

Cite this: *RSC Advances*, 2013, **3**, 4434

Received 13th November 2012,
Accepted 21st January 2013

DOI: 10.1039/c3ra22880k

www.rsc.org/advances

The reflection, transmission and absorbance spectra of silicon nanowire arrays (NWAs), as a function of the length of the nanowires, are investigated in a wavelength range of 15 μm $< \lambda <$ 200 μm, using Fourier transform infrared spectroscopy in vacuum. The NWAs are fabricated using metal-assisted electroless chemical etching. The wire length is varied between 20 μm and 140 μm, which is of the same order of magnitude as the wavelength, and their spectra are compared to bulk Si. At high frequencies the absorbance spectra of the NWAs show molecular resonances due to adsorption of molecules involved in the fabrication process but also due to the oxide quality that wraps the nanowires and changes as a function of nanowire length. Transmission characteristics show an increasing shift in absorption band edge towards the far infrared for longer wires and a transition from specular to diffuse reflection at a nanowire length of approximately 60 μm.

Introduction

Due to technological advancements in semiconductor fabrication processes and the need for smaller dimensions in different semiconductor technologies, the study of the behaviour of semiconductor nanomaterials, including nanowires and nanodots, has expanded exponentially over the last decade. Nanomaterials offer different physical properties compared to their bulk counterpart and these can be exploited in optical and/or electrical applications. Silicon nanowires (NWs) have attracted much attention due to their potential application in nanoelectronics, photonics, energy, and biosensors.[1] A variety of methods exist to fabricate NWs, including chemical techniques such as chemical vapour deposition, chemical etching, solution growth and physical techniques such as laser ablation and thermal evaporation. Of these techniques, the metal-assisted electroless chemical etching (MACE)[2] offers a simple way to prepare large-area arrays with a high density of long vertically upstanding NWs, which can lead to low cost and large scale commercial applications. The MACE method is based on Ag-induced excessive local oxidation and dissolution of a Si wafer underneath a metal in an aqueous fluoride solution. Different approaches of the MACE technique have already been presented in literature.[3] In the approach taken in this research the deposition of the Ag nanoparticles and the etching of the nanowires was done in 1 step. A bulk p-type Si sample with an area of 1.5 cm × 1.5 cm and a resistivity of ρ = 10–20 Ω cm was immersed in a wet chemical solution consisting of HF/$AgNO_3$/NH_4NO_3 with molar ratio of 5.6 M/0.03 M/0.006 M. After etching, the residual Ag particles are removed using a highly concentrated HNO_3 solution, followed by a DI water rinse. The back of the wafers is protected by PMMA (poly-methylmethacrylate) to avoid etching NWs on both sides. PMMA was removed using acetone and the samples were left to dry in ambient conditions.

The diameter of the NWs in the array varies between 30 and 300 nm. Different lengths of NWs are obtained by controlling the etch time. 20, 50, 100 and 140 μm lengths were etched during a time of respectively 1/2, 2, 5 and 6.5 h. The SEM image of a 50 μm nanowire array (NWA), fabricated using MACE, is given in Fig. 1(a). The observed wires are crystalline. The roughness at the NWA/bulk interface is clearly visible. This roughness increases with increasing etch time. Fig. 1(b) and (c) give the SEM cross section at the NWA/bulk boundary of a 20 μm and 100 μm NWA. The roughness increases from approximately 100 nm for short etch times to approximately 10 μm for longer etch times. The interface roughness is strongly dependent on the availability of Ag particles at the end stage of the etch process.[4]

Recently, Si NWAs with short NW length, fabricated with the MACE technique, have been investigated for the use in solar cells.[5] The main purpose for these short (~4 μm) NWAs is the reduction of the reflection of incoming light which increases the efficiency of Si solar cells. These measurements are done in a limited wavelength range from 0.4 μm to 1.2 μm, covering mainly the optical spectrum.

In this manuscript, we extend the transmission/reflection research on MACE-fabricated Si NWAs to cover the IR region from 14 μm to 500 μm, with the purpose of investigating the

[a]*Department of Electrical and Electronic Engineering, Imperial College London, Exhibition Road, London, SW7 2AZ, United Kingdom.*
E-mail: k.fobelets@imperial.ac.uk; Fax: +44 2075946308; Tel: +44 2075946308
[b]*State Key Laboratory on Integrated Optoelectronics, Institute of Semiconductors, Chinese Academy of Sciences, P.O. Box 912, Beijing, 100083, P. R. China*
[c]*Laboratoire Charles Coulomb, UMR 5221, CNRS-Université Montpellier 2, Montpellier, 34950, France*

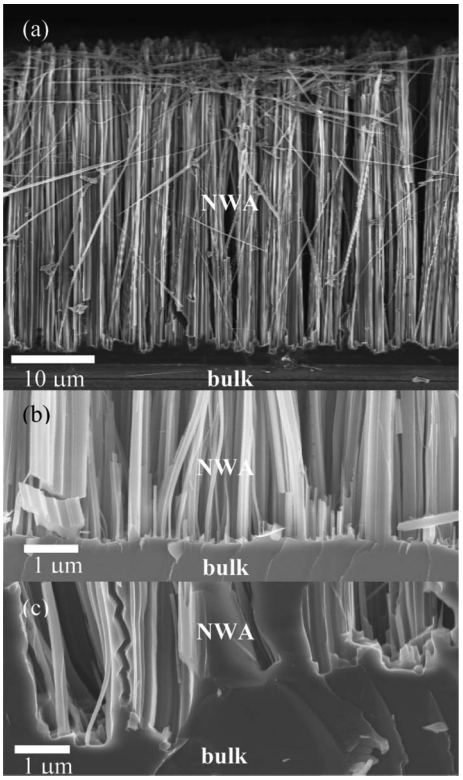

Fig. 1 SEM images of the cross section of NWAs fabricated *via* a 1-step MACE process. (a) 50 μm long NWA on bulk, (b) the NWA/bulk interface for the 20 μm NWA and (c) the NWA/bulk interface for 100 μm NWA. The scale bar in (b) and (c) is 1 μm.

influence of the fabrication technology on the quality of the wires and to investigate the influence of the NW length and interface roughness on the spectra.

The measurements are done with a Bruker IFS 66 v/S Fourier Transform Infrared (FTIR) spectrometer with different sources, beam splitters and detectors for the different wavelength ranges. FTIR is an established method in semiconductor manufacturing to analyse the quality of semiconductor wafers. Addition of different atoms or molecular species to the sample will change the transmission or reflection spectra of the material. The introduction of non-Si material will give a unique combination of atoms which vibrate at specific frequencies and thus generate additional absorption peaks that are characteristic of the new functional groups.[6] The amplitude of the peaks is indicative of the density of vibrating functional groups. The MID-IR frequency range between 500 cm^{-1} and 4000 cm^{-1} is of particular interest for this analysis. FTIR measurements for heavily doped (111) Si MACE fabricated NWAs, with and without post-HF treatment, have been presented in ref. 7. In our measurements, we investigate the variation of the adsorbed molecules as a function of NW length for lowly doped (100) Si.

In addition, the wavelength range: 14 μm $< \lambda <$ 200 μm is used to investigate both reflection and transmission as a function of nanowire length. This investigation shows a shift in the absorption band edge with length of the nanowires in the array. The influence of the NWA surface and NWA/bulk roughness is discussed.

Molecular characteristics of the nanowire array

In this section we study the material quality of the MACE fabricated NWAs. Transmission measurements were carried out on bulk Si and four NWA samples with different lengths, fabricated from the same wafer and with the same etch recipe. The average length of the nanowires in each array is 20, 50, 100 and 140 μm. The spectra were taken in a wavenumber range of 7500 $cm^{-1} > \nu >$ 360 cm^{-1}. The FTIR source used is a Globar, the beam splitter KBr and the diaphragm aperture is set at 6 mm. The measurements are done in vacuum at room temperature.

Transmission measurements can be done with different orientations of the NWA sample: with the NWA side or the bulk surface towards to incoming EM (electro-magnetic) wave. Both spectra show similar features but the spectrum with the NWA as input surface shows lower transmission amplitude due to scattering. All measurements are normalised to the reference spectrum of the Globar source. The spectra of the bulk and the 20 μm NWA sample show interference patterns related to the bulk cavity. These interference patterns disappear for longer NWAs due an increase in surface roughness of the NWA/bulk interface (see Fig. 1(b), (c)). The transmission amplitude decreases for increasing NW length by a factor of 100 for NWAs longer than 20 μm. In order to evaluate the difference between the bulk spectrum and the NWA spectra, the absorbance is calculated for the NWA spectra using the bulk as reference following:

$$\text{Absorbance} = -\ln\left(\frac{T_{\text{NWA}}}{T_{\text{bulk}}}\right) \quad (1)$$

with $T_{\text{NWA(bulk)}}$ the transmission spectra of the NWAs (bulk). The absorbance spectra of the NWAs are given in Fig. 2. The interference peaks in the bulk spectrum will impose small periodic variations on the absorbance spectra, these are much smaller than the relevant absorption peaks. The absorbance spectra for all NWAs are similar, and thus indicative of the ab-/adsorbed species on the surface of the wires in the array rather than a function of the NW length. The absolute value of the absorbance spectra should not be used because the scattering at the NWA surface influences the total transmission intensity. The relative heights of the peaks are a measure for the number of ab-/adsorbed species.

The broad absorbance peak at wave numbers in the range of 3400–3200 cm^{-1} can be attributed to Si–OH groups[8] and hydrogen bonded molecular water.[9] This molecular spectrum points towards absorption of water in the NWA. The amplitude of the absorption increases with increasing NWA length consistent with the larger available surface area that can retain a larger volume of molecular water. It has already been

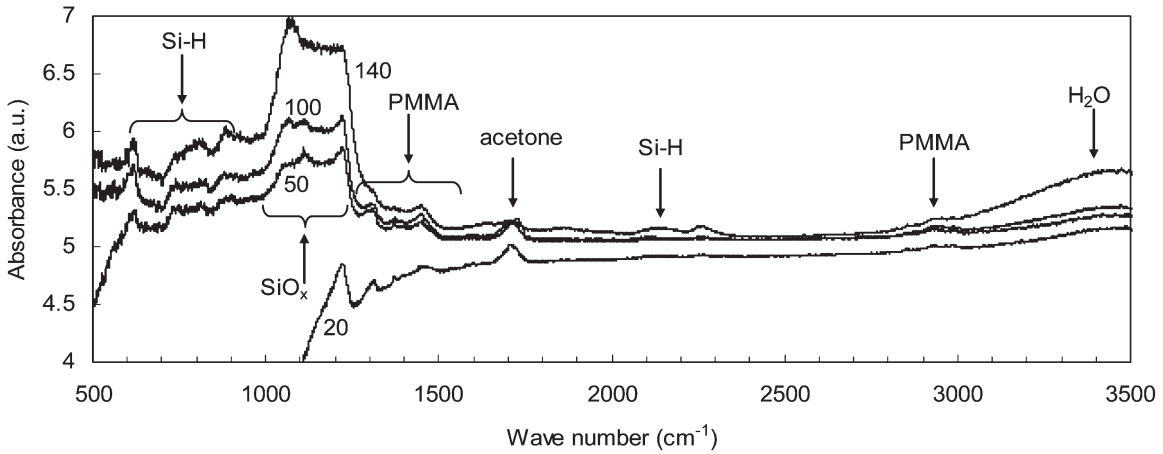

Fig. 2 Absorbance spectra of the 20, 50, 100 and 140 μm NWA. Arrows indicate the different absorption peaks. The numbers in the figure identify the NW length.

reported that the electrical characteristics of a Si NWA are influenced by air humidity.[10] The tendency of Si NWAs to retain H_2O within its structure show that for sensing application the lengths of the NWs should be kept short to avoid excessive H_2O retention.

The shallow peak at $\sim$3000 cm^{-1} is in the region of the CH_2, CH_3 stretching absorption band and can be attributed to the PMMA used to protect the back side of the Si wafer during etching. This is strengthened by the absorption peaks in the 1350–1460 cm^{-1} region which relates to the CH_2, CH_3 bending absorption band.[11] The 1740–1680 cm^{-1} band and 1710 cm^{-1} can be related to C=O stretching modes. PMMA could also influence the absorbance in this band around 1730 cm^{-1}.

An absorption peak occurs at $\sim$1700 cm^{-1}, indicating a hydrogen-bonded carbonyl band rather than a non-bonded carbonyl band associated to PMMA.[12] Carbonyl stretching modes of ketones *e.g.* acetone or carboxylic acid dimers, occur in this frequency band. In the fabrication process acetone is used to remove PMMA from the NWAs but not for the bulk sample. As a consequence the absorption peak around 1700 cm^{-1} can be associated to acetone used in the process.

Small Si–H absorption peaks are observed in the lower frequency range[13,14] 610–900 cm^{-1} for all NWA samples (except the 20 μm NWA), showing that some fraction of the Si NW surface is –H terminated after the etching process. Two additional small absorption peaks occur at $\sim$2240 cm^{-1} and $\sim$2120 cm^{-1} for the longest NWA only. These peaks can also be associated to Si–H groups but do not occur for the other NWA samples. Some indication exists that these peaks might be associated with porous silicon.[15] This means that the character of the NWs in the arrays changes as a function of etch time. Thus for longer wires the concentration of NWs of porous character in the array is increasing relative to the density of crystalline NWs. A change in the character of the wire as a function of nanowire length has also been observed by electrical conductivity measurements.[16]

The pronounced absorption band in the frequency range between 1100 and 1221 cm^{-1} can be attributed to the growth of a SiO_x layer.[17] The oxide related absorption peak increases with an increase in the length of the NWs in the array. This indicates a larger overall fraction of oxide but not necessarily a larger thickness of oxide per NW as a function of NW length. However, a shift of the main absorption peak from 1220 cm^{-1} for the shorter wires to 1060 cm^{-1} for the longest wires, is observed. An oxide absorption peak at $\sim$1200 cm^{-1} has been attributed to the longitudinal optical phonon mode of thin native oxides[13] associated to the growth of oxides nucleating on Si–OH bonds. The position of this peak shifts as a function of the surface coverage of the nucleated oxide. An absorption peak at $\sim$1050 cm^{-1} is due to Si–O stretching in thin native oxides that is sufficiently thick to be observed in the IR region. Thus the 1060 cm^{-1} peak leads us to conclude that the longer NWAs might have a thicker oxide layer than the shorter NWAs. This implies that longer etch times lead to thicker oxide layers on the surface of the Si nanowires. This observation is corroborated by the results in ref. 7 where similar modes were observed and associated to a thick native oxide layer and porous Si.

Finally, there are no consistent peaks associated to the Ag used in the process, indicating an effective removal of the Ag catalyst.

The important conclusions concerning the absorption spectra are that residue of solvents used in the fabrication process are retained for a long time in the NWA structure; that the NWAs have a natural tendency to absorb water from the atmosphere and that the longer wires have increased oxide thickness and become more porous when etched in the same solution as the shorter wires. The oxide-related absorption peak is stronger than those related to Si–H bonds, this is consistent with the fact that the long NWAs tend to be more hydrophilic after etch while the short NWAs tend to be more hydrophobic.

Optical reflection and transmission

Transmission and reflection spectra are measured in a wavelength range of 14 μm $< \lambda <$ 200 μm. This wavelength

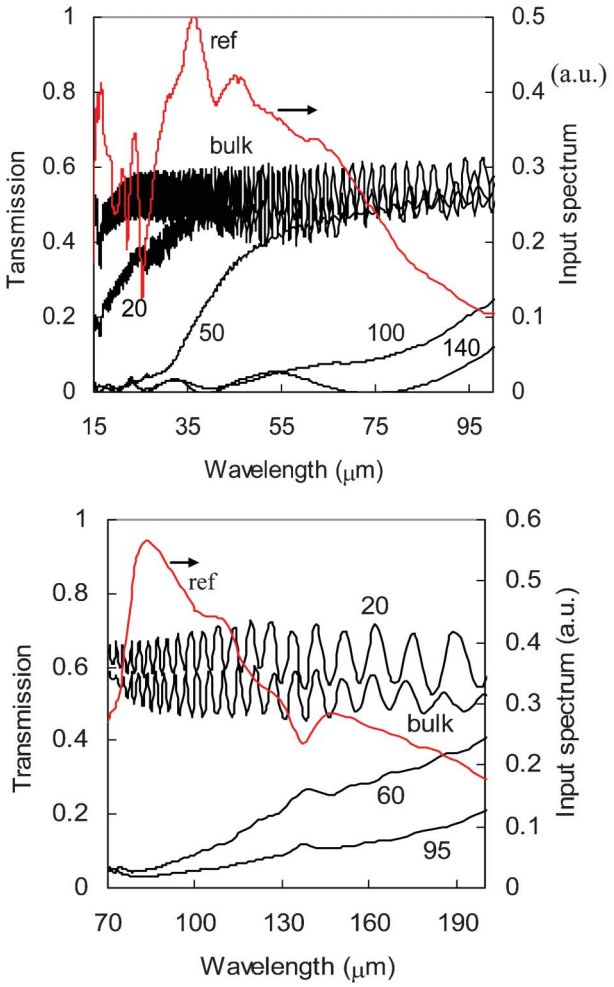

Fig. 3 Transmission spectra as a function of wavelength for bulk and NWAs. The input spectrum is given on the right axis in a.u. Top: range (1) on 20, 50, 100 and 140 μm NWA, bottom: range (2) on 20, 60 and 95 μm NWA.

range is of the same order of magnitude as the length of the NWs in the arrays. For 14 μm $< \lambda <$ 100 μm the source is a Globar, the beam splitter is 6 μm Mylar and the detector is DTGS-PE. For 70 μm $< \lambda <$ 200 μm, a Mercury source, a 23 μm beam splitter and a cooled bolometer are used. All measured spectra are normalised to the measured input spectrum of the sources.

For 14 μm $< \lambda <$ 100 μm (range (1)) the spectra of the samples have been taken with 2 sample orientations: (a) polished bulk side oriented towards the incoming EM wave and (b) NWA pointing towards the incoming EM wave. For transmission measurements the incident wave is perpendicular to the substrate. In Fig. 3, the transmission spectra, $T(\lambda)$ in both orientations are similar but with reduced amplitude in (b) due to increased scattering on the NWA surface. The transmission characteristics can be clearly divided into two groups: those for NWA lengths smaller than 60 μm and those equal and larger than 60 μm.

In the first group, the Fabry-Perot resonances of the bulk are maintained due to the relatively small bulk/NWA roughness. For these NWA lengths, reflection at the interfaces remains specular. The distance between the peaks is related to the thickness of the sample, following:

$$\Delta\lambda = \lambda_2 - \lambda_1 = \frac{\lambda_1 \times \lambda_2}{2\, n\, d} \qquad (2)$$

with λ_1, λ_2 two consecutive transmission peaks, n index of refraction and d thickness of the sample. Ignoring the change in average index of refraction of the NWA/air composite, the thickness of the bulk structure remaining in the samples, extracted from the interference fringes, is 365, 333 and 311 μm for bulk, 20 and 50 μm NWA respectively. This remaining bulk thickness is in agreement with the SEM measurements of the length of the NWAs. For NWAs longer than 60 μm, $T(\lambda)$ becomes very small, especially at shorter wavelengths. This small transmission is independent of the side on which the EM waves are impinging and is attributed to the increased NWA/bulk roughness which causes diffuse scattering and thus dramatically reduces the part of the transmitted beam falling onto the detector.

The reflection spectra, $R(\lambda)$, given in Fig. 4, are measured under a small angle of incidence of $\theta = 8^\circ$. Due to the complex input spectrum in the lower wavelength range an additional peak occurs around $\lambda \approx 26.5$ μm, this wavelength should be disregarded in the response. For reflection, the response to input orientation (a) and (b) is different, mainly due to the slight off-axis orientation of the incoming beam. As in $T(\lambda)$, $R(\lambda)$ for the 20(a) and 50(a) μm NWAs still shows interference fringes and thus a large degree of specular reflection. Interference fringes disappear for longer wires due to diffuse reflection at the increasing NWA/bulk interface roughness. $R(\lambda)$ is found to be lower for all NWA samples compared to bulk in both sample orientations. For sample orientation (a), $R(\lambda)$ is independent of NWA length. Simple calculations for TE input waves show that this decrease is the result of a decreased refractive index of the NWA/air composite near the NWA/bulk boundary. For orientation (b), $R(\lambda) \approx 0$ for the lower wavelengths due to both diffuse scattering as well as increased trapping of the waves within the NWA for off-axis irradiation. Note that the wavelength range over which $R(\lambda)$ remains small increases with increasing NWA length.

At low wavelengths, $\lambda <$ 55 μm, $T(\lambda)$ is small and then increases rapidly with increasing λ. The wavelength for the sudden onset of transmission increases with increasing nanowire length. A similar change cannot be observed in $R(\lambda)$ in neither sample orientation. Therefore, the sudden change in the transmission characteristic is associated to an increased absorption bandwidth, $A(\lambda)$ following, to first approximation: $A(\lambda) = 1 - T(\lambda) - R(\lambda)$. $A(\lambda)$ cannot be calculated for the experimental data because of the small difference in input angle for $T(\lambda)$ and $R(\lambda)$ measurements and the transition from specular to diffuse scattering. The absorption edge of Si bulk is at $\lambda_e \approx 1$ μm. For the NWA samples the absorption edge moves towards higher wavelengths, $\lambda_e \approx 5$ μm for the 20 μm NWAs and $\lambda_e \approx 40$ μm for the 50 μm NWAs. Small shifts in the absorption edge with

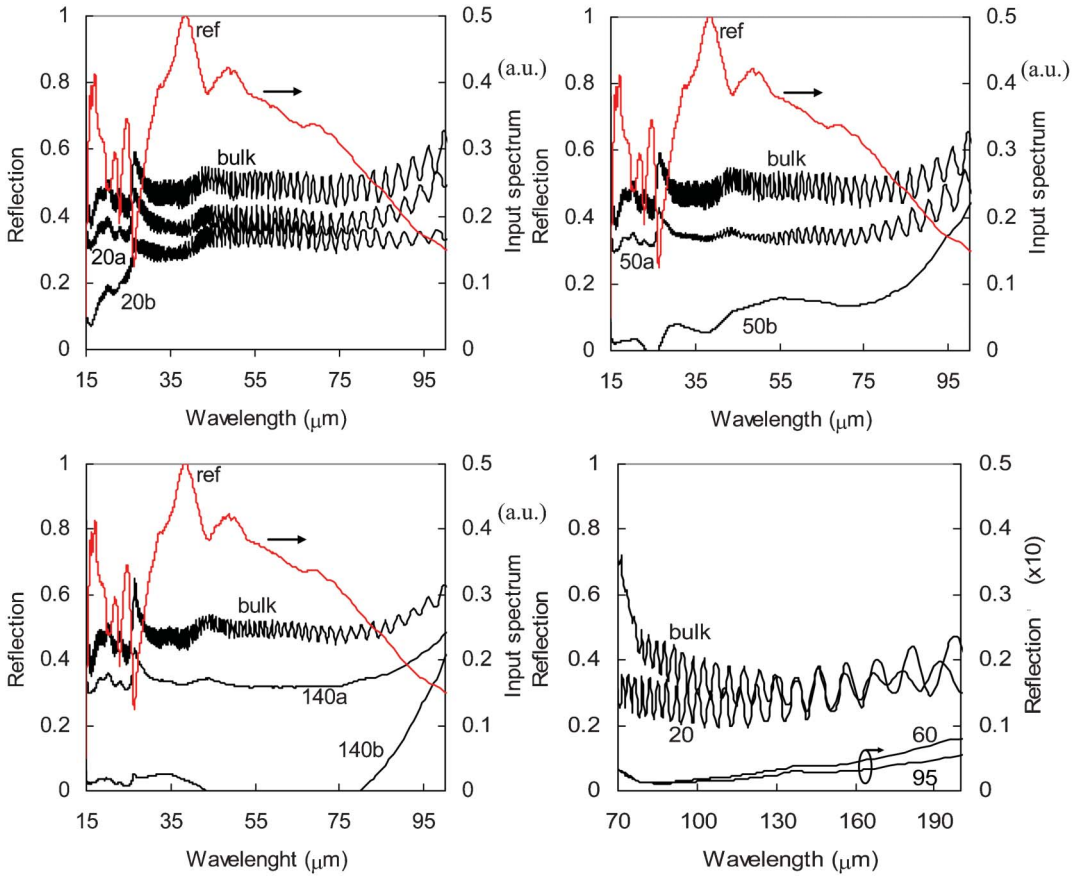

Fig. 4 Reflection spectra as a function of wavelength for bulk and NWAs for EM wave input on different sides of the sample. The numbers correspond to the NWA length, while the labels a and b refer to the input beam orientation. (a) Input beam on the polished side ; (b) input beam on the NWA side. The input spectrum is given on the right axis in a.u. Bottom right: reflection spectrum at higher wavelengths measured using a cooled bolometer detector.

nanowire length have been observed for very short periodic NWAs (1–5 μm).[18] Our measurements demonstrate that a large increase of the absorption bandwidth can be obtained by increasing the NW length to tens of μm, up to lengths of 50 μm, in non-periodic NWAs with variable wire thickness (30 nm–300 nm). This can be exploited in nanowire based hybrid solar cells to increase the wavelength range in which Si absorbs electromagnetic radiation, leading to higher efficiencies.[19]

For 70 μm $< \lambda <$ 200 μm (range (2)), measurements are presented with the EM wave impinging on the NWA side only. Measurements in range (2), using a cooled bolometer for increased detection sensitivity, show that the reflection of the long NWAs remains close to zero over a large wavelength range.

The main conclusions of this section are that the NWA/bulk interface remains sufficiently smooth for specular reflection up to a NW length of 50 μm. For these NW lengths, the absorption edge shifts to higher wavelengths with increasing length. A dramatic change in the transmission characteristics occurs from a NW length of 60 μm upwards, the light scattering process becomes diffuse due to the increasing NWA/bulk boundary roughness.

Conclusions

NWAs of different length between 20 and 140 μm, fabricated *via* metal assisted electroless etching, were characterised using Fourier Transform Infrared Spectroscopy under vacuum.

It was shown that molecular H_2O remains adsorbed within the NWAs even under vacuum conditions. Similarly, materials used in the fabrication process tend to remain within the NWA matrix, indicating that careful cleaning and drying is necessary to obtain ''pure'' NWAs. The surface states of the wires are mainly related to hydroxyl groups. The density of porous NWs increases for longer wires which also have a thicker SiO_2 layer. These features have a strong impact on the use of long Si NWA for sensing applications as the surface state of the NWs will influence the electrical characteristics of the array.

The character of the transmission spectra changes dramatically at a NWA length of 60 μm due to diffuse reflection which is a consequence of the increased roughness at the NWA/bulk interface. For NWAs shorter or equal to 50 μm, the optical absorption edge shifts towards higher wavelengths with increasing NWA length and reflection is lower than for bulk. For NWAs longer and equal than 60 μm, diffuse reflection in the NWA over the FIR wavelength range prevents

the penetration of the electromagnetic wave into the sample. Thus, increasing the length of the NWA will increase the spectral absorption range for Si NW-based solar cells. However, the maximum NW length is limited to <60 μm, for the given etch recipe, due to the increase in diffuse reflection.

Acknowledgements

This work was supported by the *e-on* International Research Initiative project. K. F. thanks J. Łusakowski for useful discussions.

References

1 (*a*) V. Schmidt, J. V. Wittemann, S. Senz and U. Gösele, *Adv. Mater.*, 2009, **21**, 2681; (*b*) M. Shao, D. D. D. Ma and S.-T. Lee, *Eur. J. Inorg. Chem.*, 2010, 4264; (*c*) L. J. Chen, *J. Mater. Chem.*, 2007, **17**, 4639–4643.

2 (*a*) K. Q. Peng, Y. Wu, H. Fang, X. Y. Zhang, Y. Xu and J. Zhu, *Angew. Chem., Int. Ed.*, 2005, **44**, 2737; (*b*) K. Q. Peng, J. J. Hu, Y. J. Yan, Y. Wu, H. Fang, Y. Xu, S. T. Lee and J. Zhu, *Adv. Funct. Mater.*, 2006, **16**, 387; (*c*) Z. Huang, N. Geyer, P. Werner, J. de Boor and U. Gösele, *Adv. Mater.*, 2011, **23**(2), 285–308.

3 (*a*) M. L. Zhang, K. Q. Peng, X. Fan, J. S. Jie, R. Q. Zhang, S. T. Lee and N. B. Wong, *J. Phys. Chem. C*, 2008, **112**, 4444; (*b*) Y. Q. Qu, L. Liao, Y. J. Li, H. Zhang, Y. Huang and X. F. Duan, *Nano Lett.*, 2009, **9**, 4539; (*c*) Z. P. Huang, H. Fang and J. Zhu, *Adv. Mater.*, 2007, **19**, 744.

4 C. Li, *Internal report*, EE Dept., Imperial College London, 2012.

5 (*a*) K. Peng, Y. Xu, Y. Wu, Y. Yan, S.-T. Lee and J. Zhu, *Small*, 2005, **1**, 1062; (*b*) D. Kumar, S. K. Srivastava, P. K. Singh, M. Husain and V. Kumar, *Sol. Energy Mater. Sol. Cells*, 2011, **95**, 215; (*c*) S. K. Srivastava, D. Kumar, P. K. Singh, M. Kar, V. Kumar and M. Husain, *Sol. Energy Mater. Sol. Cells*, 2010, **94**, 1506–1511; (*d*) Y.-A. Dai, H.-C. Chang, K.-Y. Lai, C.-A. Lin, R.-J. Chung, G.-R. Lin and J-H. He, *J. Mater. Chem.*, 2010, **20**, 10924–10930; (*e*) H. Chen, R. Zou, H. Chen, N. Wang, Y. Sun, Q. Tian, J. Wu, Z. Chen and J. Hu, *J. Mater. Chem.*, 2011, **21**, 801–805.

6 G. Lopinski, *Int. J. Nanotechnol.*, 2008, **5**, 1247.

7 V. A. Sivakov, F. Voigt, A. Berger, G. Bauer and S. H. Christiansen, *Phys. Rev. B: Condens. Matter Mater. Phys.*, 2010, **82**, 125446.

8 P. J. Launer, in *Infrared Analysis of Organosilicon Compounds: Spectra-Structure Correlations, Silicon Compounds and Review*, ed. B. Arkles, Petrach System, 1987, p.100.

9 M. Nogami and Y. Abe, *Phys. Rev. B: Condens. Matter*, 1997, **55**, 12108.

10 G. Dubey and G. P. Lopinski, *Appl. Phys. Lett.*, 2007, **91**, 232111.

11 L. Ling, S. Kuwabara, T. Abe and F. Shimura, *J. Appl. Phys.*, 1993, **73**, 3018.

12 J. Dong and Y. Ozaki, *Macromolecules*, 1997, **30**, 386.

13 A. Hiraki, T. Imura, K. Mogi, M. Tahiro and J. de Physique, *Colloque C4*, 1981, **10**, 62–277.

14 N. B. Colthup, L. H. Daly and S. E. Wiberley, in *Introduction to infrared and Raman spectroscopy,* Academic Press, New York-London, 1964.

15 D. B. Mawhinney, J. A. Glass and J. T. Yates, *J. Phys. Chem. B*, 1997, **101**, 1202.

16 M. Zaremba-Tymieniecki, C. B. Li, K. Fobelets and Z. A. K. Durrani, *IEEE Electron Device Lett.*, 2010, **31**, 860.

17 L. Ling, S. Kuwabara, T. Abe and F. Shimura, *J. Appl. Phys.*, 1993, **73**, 3018.

18 L. Hu and G. Chen, *Nano Lett.*, 2007, **7**, 3249.

19 (*a*) B. Tian, X. Zheng, T. J. Kempa, Y. Fang, N. Yu, G. Yu, J. Huang and C. M. Lieber, *Nature*, 2007, **449**, 885–889; (*b*) Z. Fan, H. Razavi, J.-W. Do, A. Moriwaki, O. Ergen, Y.-L. Chueh, P. W. Leu, J. C. Ho, T. Takahashi, L. A. Reichertz, S. Neale, K. Yu, M. Wu, J. W. Ager and A. Javey, *Nat. Mater.*, 2009, **8**, 648–653.